Faraday Discussions

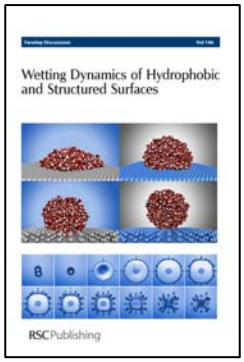

This paper is published as part of Faraday Discussions volume 146: Wetting Dynamics of Hydrophobic and Structured Surfaces

Introductory Lecture

Papers

Discussion

Papers

Molecular dynamics simulations of urea–water binary droplets on flat and pillared hydrophobic surfaces
Takahiro Koishi, Kenji Yasuoka, Xiao Cheng Zeng and Shigenori Fujikawa, *Faraday Discuss.*, 2010
DOI: 10.1039/b926919c

Discussion

General discussion
Faraday Discuss., 2010
DOI: 10.1039/c005416j

Papers

First- and second-order wetting transitions at liquid–vapor interfaces
K. Koga, J. O. Indekeu and B. Widom, *Faraday Discuss.*, 2010
DOI: 10.1039/b925671g

Hierarchical surfaces: an *in situ* investigation into nano and micro scale wettability
Alex H. F. Wu, K. L. Cho, Irving I. Liaw, Grainne Moran, Nigel Kirby and Robert N. Lamb, *Faraday Discuss.*, 2010
DOI: 10.1039/b927136h

An experimental study of interactions between droplets and a nonwetting microfluidic capillary
Geoff R. Willmott, Chiara Neto and Shaun C. Hendy, *Faraday Discuss.*, 2010
DOI: 10.1039/b925588e

Hydrophobic interactions in model enclosures from small to large length scales: non-additivity in explicit and implicit solvent models
Lingle Wang, Richard A. Friesner and B. J. Berne, *Faraday Discuss.*, 2010
DOI: 10.1039/b925521b

Water reorientation, hydrogen-bond dynamics and 2D-IR spectroscopy next to an extended hydrophobic surface
Guillaume Stirnemann, Peter J. Rossky, James T. Hynes and Damien Laage, *Faraday Discuss.*, 2010
DOI: 10.1039/b925673c

Discussion

General discussion
Faraday Discuss., 2010
DOI: 10.1039/c005417h

Papers

The search for the hydrophobic force law
Malte U. Hammer, Travers H. Anderson, Aviel Chaimovich, M. Scott Shell and Jacob Israelachvili, *Faraday Discuss.*, 2010
DOI: 10.1039/b926184b

The effect of counterions on surfactant-hydrophobized surfaces
Gilad Silbert, Jacob Klein and Susan Perkin, *Faraday Discuss.*, 2010
DOI: 10.1039/b925569a

Hydrophobic forces in the wetting films of water formed on xanthate-coated gold surfaces
Lei Pan and Roe-Hoan Yoon, *Faraday Discuss.*, 2010
DOI: 10.1039/b926937a

Interfacial thermodynamics of confined water near molecularly rough surfaces
Jeetain Mittal and Gerhard Hummer, *Faraday Discuss.*, 2010
DOI: 10.1039/b925913a

Mapping hydrophobicity at the nanoscale: Applications to heterogeneous surfaces and proteins
Hari Acharya, Srivathsan Vembanur, Sumanth N. Jamadagni and Shekhar Garde, *Faraday Discuss.*, 2010
DOI: 10.1039/b927019a

Discussion

General discussion
Faraday Discuss., 2010
DOI: 10.1039/c005418f

Concluding remarks

Concluding remarks for FD 146: Answers and questions
Frank H. Stillinger, *Faraday Discuss.*, 2010
DOI: 10.1039/c005398h

Dynamical superhydrophobicity

Mathilde Reyssat,†[a] Denis Richard,[a] Christophe Clanet[ab] and David Quéré[ab]

Received 7th January 2010, Accepted 10th February 2010
DOI: 10.1039/c000410n

Superhydrophobicity is mainly remarkable for the special dynamical behaviours it generates: low adhesion, giant hydrodynamic slip, frictionless motion, rebounds after impacts. Here we discuss most of these properties. We first recall how contact angle hysteresis can be minimized in this state. Then, we show that a water drop first follows the Galilean law of free fall on an incline, before reaching a stationary state, for which we discuss the associated friction. Finally, the property of water repellency (that is, rebounds after impact) is presented. We describe in particular how the texture responsible for superhydrophobicity can also influence the figure of impact at a very large scale.

1. Introduction

When placed on a very hot plate, a drop of water levitates, owing to the formation of a vapour film that prevents the contact between the liquid and its substrate. This situation, often referred to as the Leidenfrost phenomenon,[1] is characterized by its remarkable mobility: suppressing the solid/liquid contact minimizes the viscous force associated with the drop motion, which is just resisted by the inertial friction arising from the presence of air around, as for a free-falling raindrop. The absence of a solid/liquid contact can be viewed as the ultimate hydrophobic state, where the "contact" angle reaches 180°, its maximum possible value.

At room temperature, water evaporation is much reduced but materials may approach the Leidenfrost limit if they are covered with a hydrophobic texture (typically at a scale of 100 nm to 10 μm), which acts as a spacer between the liquid and the solid (Fig. 1). The larger the quantity of air trapped in the textures, the larger the contact angle: water makes contact angles of the order of 160 to 175° on many natural[2] or artificial[3] materials of this kind. In addition, the hysteresis of contact angle is generally very low (about 5 to 10°) in this "fakir regime", since the drop can only pin on the few texture tops it contacts. As a consequence, liquid adhesion is highly reduced compared to usual materials.[4] Interestingly, special designs can also provide superoleophobicity, *i.e.* the possibility for a deposited oil to find an equilibrium position on the texture tops, leaving air trapped below.[5]

In a superhydrophobic situation, the liquids dynamics dramatically differs from what is known for usual materials, as demonstrated by three original effects: (i) A huge slip can be observed at the frontier between the liquid and the solid, when displaced relative to each other: the associated slip length can be more than 1000 times larger than on a hydrophobic flat material.[6] The magnitude of the slip depends on the design of the texture and on the pressure applied on the liquid. Research on slip has been particularly active for the last five years, and a recent comprehensive

[a]*PMMH, ESPCI, 10 rue Vauquelin, 75005 Paris, France*
[b]*LADHYX, École Polytechnique, 91128 Palaiseau Cedex, France*

† Current address: MMN, Gulliver, ESPCI, 10 rue Vauquelin, 75005 Paris, France.

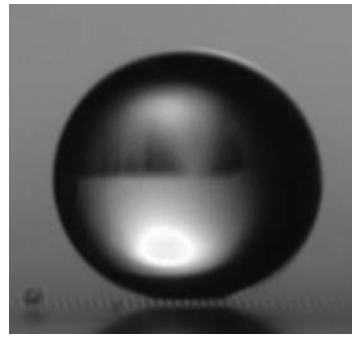

Fig. 1 A water drop deposited on a bed of hydrophobic micronails often stays at the top of the nails. This is directly observed in this photo, where the low density of nails (about 1%) together with the presence of air allows light to pass below the drop (of diameter 0.8 mm). The distance between the drop and its reflection is 24 μm, that is, twice the height of the micropillars used in this experiment. We discuss in this paper the dynamical properties generated by such a "fakir state".

review by Rothstein summarizes the main findings on this subject.[7] (ii) A second effect, first qualitatively reported by Leidenfrost who had to use (hot) spoons to trap drops,[1] is the remarkable mobility of pearl drops. On superhydrophobic solids, mobility arises from the conjunction of small hysteresis, which minimizes the force anchoring the liquid on its substrate, and low friction, as the drop moves.[8–11] Remarkably, very little was reported on the latter effect, and it is one of our primary goals here to discuss possible origins and magnitude for this friction. We also recall how contact angles and their hysteresis can be deduced from the density of the textures placed on the solid. (iii) The third spectacular effect generated by superhydrophobic materials is, literally, water repellency: when thrown on such materials, water bounces off, leaving the substrate dry after the rain.[12–15] We describe a few characteristics of these rebounds, and present new experiments where impact is accompanied by remarkable patterns directly related to the existence of a texture on the solid surface.

2. Residual drop adhesion

We first consider the question of pinning, for a drop of radius R made of a liquid of surface tension γ and density ρ, and deposited on an incline. We classically define the capillary length κ^{-1} as $\sqrt{\gamma/\rho g}$, that is, 2.7 mm for water. We mainly consider drops smaller than κ^{-1}, *i.e.* whose behaviour is dictated by surface tension rather than by gravity. The reason why such drops do not move on inclines is often visible with a naked eye: the angle at the leading edge is larger than the one at the trailing edge, which generates a Laplace pressure difference opposing gravity.[16] This asymmetry is clearly visible in Fig. 2, where a fakir drop such as the one in Fig. 1 is tentatively displaced by a syringe contacting its top and moved laterally. Just before the drop starts moving, it is asymmetric with a leading angle θ_a significantly larger than the trailing angle θ_r.

The detailed calculation of the force resisting the motion is not easy, because of the three-dimensional character of the drop geometry: the angle continuously decreases along the contact line, when following it from the front to the rear of the drop.[17] However, a simple approximation allows us to quantify the typical magnitude of the maximum sticking force F. Assuming that half the rear of the drop meets the solid with θ_r, and that the other half meets the solid with θ_a, we deduce that F scales as $\gamma\ell(\cos\theta_r - \cos\theta_a)$, denoting ℓ as the radius of the contact

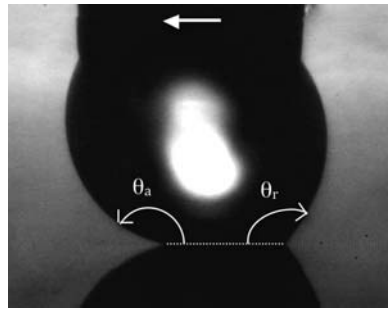

Fig. 2 A drop resists the motion that we try to impose (with a syringe, the black body on the top, of diameter 1 mm) by pinning on the substrate, which clearly generates a difference of contact angle between the leading and the trailing edge. The arrow indicates the direction of the applied force. Here the drop is in a fakir state, on a substrate decorated with hydrophobic posts of height $\delta = 20$ μm, radius $b = 1.3$ μm and mutual distance $p = 7$ μm. The advancing and receding angles θ_a and θ_r are $159 \pm 2°$ and $126 \pm 2°$, respectively. The hysteresis $\Delta\theta = \theta_a - \theta_r \approx 30°$ is significant despite the small density of pillars ($\phi \approx 10\%$).

(taken as a circle, a good approximation in the highly-hydrophobic limit).[18] For ultra-hydrophobic situations ($\theta \approx 180°$), this contact is set by gravity,[8] but in most practical situations, it is simply given by the geometric relationship: $\ell \approx R\sin\theta$, where we define the mean contact angle θ as $(\theta_r + \theta_a)/2$. Since water repellent situations are characterized by both $\Delta\theta = \theta_a - \theta_r \ll \theta$ and $\varepsilon = \pi - \theta \ll 1$, we can expand the formula for F, which yields:

$$F \sim \gamma R\, \varepsilon^2\, \Delta\theta \tag{1}$$

Hence F is smaller than a "usual" hysteresis force γR by a factor $\varepsilon^2\Delta\theta$, *i.e.* about 100 for $\varepsilon = \Delta\theta = 10°$. Only the drops verifying the inequality $F > \rho g R^3$ should remain pinned on vertical plates, that is, drops smaller than $\kappa^{-1}\varepsilon\Delta\theta^{1/2}$, instead of κ^{-1} on usual solids. This implies droplets with a radius of typically 100 μm, much smaller than the millimetre-size drops sticking on our window panes. Note however that this average-based description might fail if the drop size becomes of the order of the texture characteristic length, in which case the drop obviously can sink and remain trapped in the texture.

Eqn (1) makes it clear that an efficient superhydrophobic surface (small F) combines a high contact angle ($\varepsilon \ll 1$) and a small hysteresis ($\Delta\theta \ll 1$). It is worth noticing that both these quantities can be fixed by a single parameter, often referred to as ϕ, the proportion of solid in contact with the liquid. First, Cassie showed long ago that the contact angle on a superhydrophobic solid is an average between the angle θ_o on this solid, yet flat, and the angle on air, which is 180°.[19] The average is calculated on the surface energies, that is, on the cosines of the angles, which yields in the limit we are considering here ($\varepsilon \ll 1$):

$$\varepsilon \approx [2(\cos\theta_o + 1)\, \phi]^{1/2} \tag{2}$$

We often cannot observe trapped air, due to the small size of the textures and eqn (2) may be used to deduce the effective solid/liquid contact ϕ from the simple and direct measurement of ε.[20] For example, for $\varepsilon \approx 10°$, $\phi \approx \varepsilon^2$ is only 3% of the apparent contact between a drop and its substrate. Conversely, eqn (2) cannot always be used to predict the value of ε. On a disordered rough surface, we do not know *a priori* the value of ϕ, which results from a minimization of surface energy in a complex energy landscape.[21] Even more sneakily, ϕ can be a function of the way the drop was deposited (gently, or brutally, *etc.*).[4] In any case, a model situation

appears to be that of textures made of pillars or grooves, for which we select the value of ϕ (it is simply the density of texture), provided that the deposited liquid stays at the top of the texture.

In the pillar case, it is possible to calculate the value of the hysteresis $\Delta\theta$, *i.e.* to relate this macroscopic observation to the detail of contact line pinning on this well-defined texture. There is today no consensus on this question,[22] and we follow here the line proposed by Joanny and de Gennes, where the hysteresis $\gamma(\cos\theta_r - \cos\theta_a)$ is viewed as the energy (by unit area) stored by the contact line deformation on the defects.[23,24] The model assumes an ideal substrate decorated with a small density of defects. This condition is satisfied in the fakir picture, where the liquid sits on air (the most ideal substrate, indeed, with no kind of pinning), apart from a few pillars ($\phi \ll 1$). The contact line can be strongly pinned on the pillar edges, with a typical force per pillar (of radius b) scaling as γb. We try here to quantify how a fakir drop resists motion. Since its leading edge hardly resists, we assume that hysteresis mainly arises from the pinning of the trailing edge. On each pillar, the line and thus the liquid surface deform as we try to displace the drop, as sketched in Fig. 3.

Surface energy is stored in the deformation, but the "tongues" that develop must remain in equilibrium with the rest of the drop. For a drop much larger than the defects, we take a condition of zero Laplace pressure everywhere. Therefore the curvature of a tongue must be zero, which is feasible provided its two radii of curvature have opposite signs. As learnt from wetting menisci on thin fibers, the corresponding shapes are catenoids of equation $y \sim b\ \cosh(x/b)$, taking x as the axis along the deformation.[23] The deformation is larger than b, so that the former equation can be inverted: $x \sim b\ \ln(y/b)$, whose maximum is reached when the lateral deformation y reaches (half) the distance p between pillars. Then, we have $x \sim b\ \ln(p/b)$, typically a few times b, and the capillary force per pillar can be rewritten: $f \sim \gamma b \sim (\gamma/\ln(p/b))\ x$.

The latter formula implies a classical Hookean elastic energy (varying as x^2), with a non-classical stiffness, $\gamma/\ln(p/b)$ instead of γ, the usual stiffness in surface elasticity. At the maximum deformation, the receding angle is reached and the surface energy can be written $\gamma b^2 \ln(p/b)$. Since there is one pillar per unit area p^2, and using the definition of ϕ ($\phi \sim b^2/p^2$), the surface energy per unit area stored at the maximum deformation scales as $\gamma\phi|\ln\phi|$. We identify this expression with the definition of the hysteresis $\gamma(\cos\theta_r - \cos\theta_a)$, and expand it at small $\Delta\theta = \theta_a - \theta_r$, from which we get:[18]

$$\Delta\theta \sim \phi^{1/2}|\ln\phi| \tag{3}$$

where we used a simplified version of eqn (2) ($\varepsilon \sim \phi^{1/2}$).

As for the contact angle (eqn (2)), the hysteresis is found to be determined by the density of pillars ϕ. And similarly, both dependencies are critical in this parameter (exponent ½ in both cases, plus a slowly diverging logarithm for the hysteresis, in agreement with recent experiments[18]). These behaviours are related to the choice of pillars as a texture. Rounded defects with no sharp edges, for example, minimize

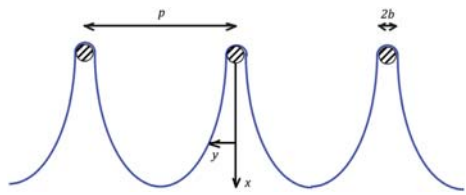

Fig. 3 Top view of the trailing edge of a fakir drop, as we try to displace it in the x-direction. The drop resists the motion by pinning on the edges of the pillars; hence a surface energy stored in this deformation, as expressed by the macroscopically observed contact angle hysteresis.

the pinning of the contact line, which should make the hysteresis vanish, as indeed observed by Gao and McCarthy.[3] Conversely, the logarithmic term in eqn (3) explains why non-negligible residual adhesion is observed in the fakir state in the limit of dilute pillars.[18,25]

Note finally that the conjunction of eqn (2) and 3 allows us to specify how the adhesion force (eqn (1)) increases as a function of the pillar density. We find $F \sim \gamma R\ \phi^{3/2}|\ln\phi|$, indicating a strong reduction of adhesion (by a factor of $\phi^{3/2}|\ln\phi|$, *i.e.* about 25 for $\phi = 5\%$), compared to usual situations ($F \sim \gamma R$). This relationship also shows how drops can be separated according to their sizes, using a substrate of spatially-decreasing ϕ. Then we expect the successive zones of the solid to stop gradually the drops, the largest ones going further on the incline.

3. Sliding pearls

A drop runs down a superhydrophobic incline (tilted by an angle α from the horizontal) if its weight $\rho g R^3 \sin\alpha$ exceeds the hysteretic force discussed in section 2.[16] Assuming this condition, we try here to understand the mobility of this drop. In the limit of zero wetting and at large viscosity, first, Mahadevan and Pomeau showed that the liquid should roll as a solid, and thus only dissipate energy by viscosity in the (tiny) Hertz zone where it contacts the solid.[8] In the limit of zero wetting ($\varepsilon = 0$), the size ℓ of the contact zone is fixed by the weight of the drop, which makes it increase as the square of its radius ($\ell \sim R^2\kappa$). Hence the surface area ℓ^2 of the contact grows as R^4, which generates a remarkable behaviour: the smaller the drops, the quicker they run down the hill![8,11]

Small viscous drops (of size $R < \varepsilon\kappa^{-1}$) on a superhydrophobic solid should behave differently. Then, the solid/liquid contact zone is the (residual) wetting contact $R\varepsilon$, larger in this limit than the gravitational contact $R^2\kappa$. At small Reynolds numbers, these drops also rotate, as proposed by Mahadevan and Pomeau.[8,9] Since viscosity η only matters in the contact zone $R\varepsilon$, the viscous force scales as $(\eta V/R)\ (R\varepsilon)^2$, denoting V as the descent velocity of the drop. V is eventually fixed by a torque balance: $\eta V R\varepsilon^2\ (R\varepsilon) \sim \rho g R^4 \sin\alpha$, which yields:

$$V \sim \frac{\rho g R^2}{\eta \varepsilon^3} \sin\alpha \tag{4}$$

This formula appears to be a kind of Stokes velocity, yet increased by a factor of $1/\varepsilon^3$, typically of the order of 100! However, it should be emphasized that this regime is expected for small drops ($R < \varepsilon\kappa^{-1}$), yet large enough to move despite the residual contact angle hysteresis, that is, for solids with a very low hysteresis.

A much more common case is that of water, of low viscosity. After rain hits water repellent materials, drops quickly run on them, taking dust and contaminants, a cleaning behaviour often referred to as the lotus effect.[26] Here we discuss the dynamics of drops of low viscosity running down superhydrophobic inclines. Let us start by an experiment. To achieve long substrates, we simply glued lycopodium grains on aluminium plates. The static contact angle of water on this solid is $165 \pm 5°$ ($\varepsilon \approx 0.25$), and the contact angle hysteresis $\Delta\theta$ is $10 \pm 5°$. The total length of the plate is 1 m, allowing us not only to follow the beginning of the descent, but also to characterize the stationary state, once gravity balances the friction acting on the liquid. This state is reached after a run of typically 1 m. The drop radius is 2 mm, large enough to overcome the hysteresis force. We first focus on the first moments of the motion ($t < 0.2$ s), and plot in Fig. 4 the position x of a millimetric water pearl deposited on the substrate tilted by $\alpha = 13°$, as a function of time t (full circles). Data are deduced from a high-speed video recording shot at 2000 frames per second.

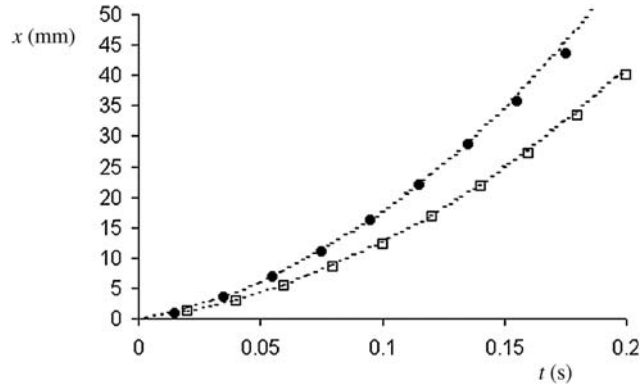

Fig. 4 Position x of a water drop on a super-hydrophobic incline tilted by $\alpha = 13°$, as a function of time t. The solid circles are the data, and the dotted line fitting them the law of free fall: $x = 1/2gt^2\sin\alpha$, with g the gravity acceleration. In the same plot, we display the position of a steel marble running down the same incline (empty squares). Because of the rotation of the marble, the law of free fall writes $x = 5/14gt^2\sin\alpha$, represented in a dotted line and found to fit the data. The water drop thus moves faster than the solid marble.

At this small scale ($x < 5$ cm, typically the scale of a leaf), the drop is observed to constantly accelerate, in agreement with earlier observations by Nakajima *et al.*[10] The trajectory is even found to be fitted by the law of free fall, $x = 1/2gt^2\sin\alpha$, drawn with a dotted line in the same plot. Friction can be neglected during the first centimetres of the run, and the motion is purely slippery. This can be confirmed by including tracers inside the drop: the tracers are just translated as the drop moves, contrasting with viscous liquids for which rotation starts immediately.[9] Superhydrophobic surfaces thus evacuate water drops as quick as possible. A drop even moves faster than a steel marble (of the same size) running down the incline (open squares in Fig. 4). Then, we also observe a constant acceleration, but the speed is smaller, for a given position, because the marble rolls. Its moment of inertia being $2/5MR^2$, with M its mass and R its radius, the law of free fall for a rolling sphere writes $x = 5/14gt^2\sin\alpha$, indeed found in Fig. 4 to fit the trajectory of the marble.

The total force acting on the drop in this regime is the weight $Mg\sin\alpha$ minus the hysteresis F. Using eqn (1) implies that the descent can be described by an effective gravity scaling as $g\,(1 - \kappa^{-2}\varepsilon^2\,\Delta\theta/R^2\,\sin\alpha)$ instead of $g\sin\alpha$. The correction is negligible in the experiment of Fig. 4, for which the number $\kappa^{-2}\varepsilon^2\,\Delta\theta/R^2\alpha$ is expected to be on the order of 5%. If we have $F \ll Mg\sin\alpha$, hysteresis slightly reduces the efficiency of the descent, but it preserves the ability of the drops to accelerate on centimetric distances. This allows these liquid pearls to reach large terminal velocities. In Fig. 5, we show how the data in Fig. 4 deviate at large scale ($x \approx 0.1$ to 1 m) from the law of free fall (still in dotted line). The drop velocity V tends towards a constant, of the order of 1 m s^{-1} in this case, despite the modest angle of inclination: drops of similar size on a vertical window pane typically move at 1 cm s^{-1}. The velocity V here is comparable to the terminal speed of a drop in air (apart from the fact that gravity is reduced by a factor $\sin\alpha$), suggesting that air friction limits the drop speed.

In the terminal state, we also observe that tracers (which were translating in the acceleration regime) now have circular trajectories inside the drop, revealing a mixture of rolling and sliding in this regime. The combination of air friction and rolling dramatically affects the drop shape (Fig. 6). First, what was a sphere at a low speed (that is, in the acceleration regime described in Fig. 4) becomes elongated. At first glance, this is natural: a tear generally leaves a trace behind it; in other words, in partial wetting, there is a threshold velocity above which liquid is

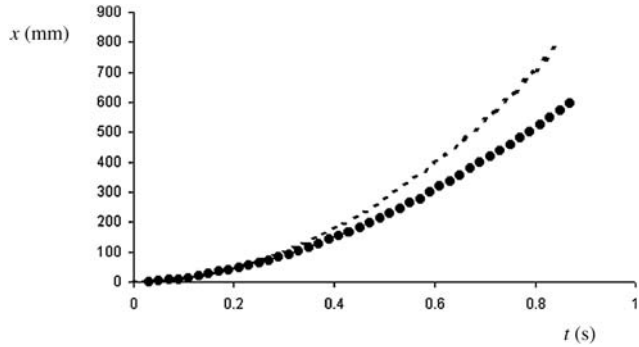

Fig. 5 At a larger scale (1 m), the trajectory deviates from the law of free fall (in the dotted line) and the water drop reaches a terminal velocity V, here of approximately 1 m s^{-1}, 100 to 1000 times larger than on a window pane, or on a tilted plastic.

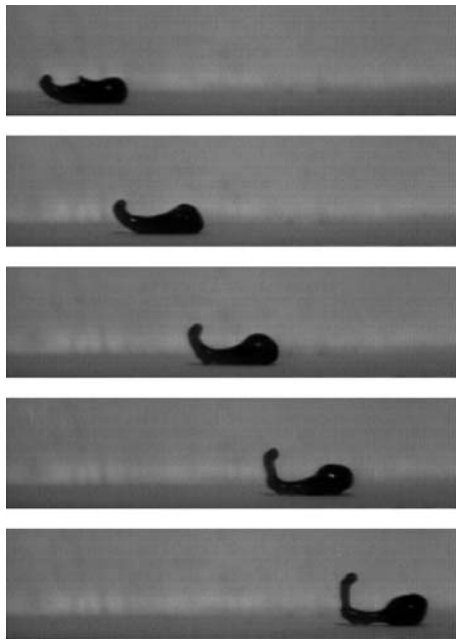

Fig. 6 Successive snapshots of a water drop (initial radius $R = 2.5$ mm) running down a superhydrophobic plate inclined by $\alpha = 60°$ (the high speed camera is tilted by the same angle, and shoots 18000 pictures per second). The picture width is 41 mm, the interval between snapshots 2.8 ms, and the drop speed $V = 2.5$ m s^{-1}. At such a high speed, a tail appears at the rear of the drop and the drop becomes a centimetre-long. Remarkably, this tail leaves the substrate, which remains dry behind the drop despite the speed.

abandoned behind the drop, because of the viscous friction at its trailing edge.[27] However, the liquid tail observed in Fig. 6 is original: it leaves the substrate, bends, and runs down at a velocity comparable to the drop speed V. This might arise from the centrifugation associated with the drop rotation: the Weber number, which compares the centrifugal force $\rho V^2/R$ to the capillary force γ/R^2 is on the order of 1 to 10 in this experiment. Since centrifugal force tends to expel liquid from the axis of rotation, *i.e.* perpendicularly to the direction of motion, the tail is indeed

likely to bend. This effect is of practical interest: as a drawback of the quick motion, the drop should abandon a trace, leaving the solid partially wet (the tail then decaying in microdroplets because of the Rayleigh instability). The bending of the tail avoids this detrimental effect.

Despite the complexity of the shape of the tumbling drop, we can add a few simple thoughts about its terminal velocity. The "natural" Reynolds number $Re = \rho_a R V/\eta_a$ (with η_a the air viscosity) being of the order 10 here, it would be "natural" to assume an inertial friction. Balancing such a force, of the form $\rho_a R^2 V^2$, with the drop weight, we immediately find the classical formula:

$$V \sim \left(\frac{\rho g R \sin\alpha}{\rho_a}\right)^{1/2} \tag{5}$$

Eqn (5) implies a descent velocity of a few meters per second, as observed experimentally. However, the drop shape does not seem to fit with this scenario: the drop elongates along the movement, which is characteristic of a viscous deformation. If inertia were dominant, the Bernoulli pressure would stretch the drop perpendicularly to the motion.[28] Our Reynolds number suggests that inertia dominates viscosity, but its construction might be too naive: drops are moving on a film of air, either trapped below the liquid, or possibly dynamically entrained by the motion itself. The large value of the static contact angle favours air entrainment,[29] generating a kind of dynamical Leidenfrost phenomenon and, subsequently, large slip.[30] If we assume a viscous friction of the order of $(\eta_a V/\delta)R^2$, where δ is the thickness of the air layer and η_a the air viscosity, we get for the descent velocity:

$$V \sim \frac{\rho g R \delta \sin\alpha}{\eta_a} \tag{6}$$

which is also expected to be a few meters per second provided that δ is in the range of 1 to 10 μm. These estimates are of course quite rough: (i) the exact law for the dissipation depends on the detail of the flow of air, either inside the texture, or as it penetrates below the drop; (ii) the drop itself can be deformed by the flow (see Fig. 6), which impacts the surface area on which the viscous stress applies. However, the typical scale for the thickness δ should indeed be micrometric, whatever the nature (*i.e.* static or dynamical) of the film. We do need a series of precise experiments to test quantitatively the scaling laws expressed in the latter equations, for example as a function of the tilting angle of the solid (see the differences between eqn (5) and 6).

If the film of air is dynamical, we can go slightly further in the analysis. For a small drop, the pressure in the film is set by the Laplace pressure γ/R and the length connecting the unperturbed drop to the film should scale as $(\delta R)^{1/2}$, as proposed by Landau and Levich. Following this line, the film thickness δ should result from a balance between viscous effects and capillary elasticity ($\eta_a V/\delta^2 \sim \gamma/(\delta^{1/2}R^{3/2})$), which yields the classical Landau–Levich scaling: $\delta \sim R\,(\eta_a V/\gamma)^{2/3}$ (or as $\kappa^{-1}(\eta_a V/\gamma)^{2/3}$ for bigger drops, for which the curvature at the front is set by the capillary length κ^{-1}). The capillary number $\eta_a V/\gamma$ is typically 10^{-3} in these experiments, which gives for the above scaling a thickness $\delta \sim 10$ μm for the air cushion. This thickness is clearly too small to be observed directly, as it can be for a Leidenfrost film ten times thicker. It is also worth noticing that δ can be comparable to the texture height, which might complicate the analysis.

4. Drop impact: from rebound to crystallographic splashing

The way superhydrophobic materials react to water drops impacts is probably the most well-known manifestation of water repellency. Provided that the capillary

number $\eta V/\gamma$ is small enough (denoting V as the impact velocity, and η as the liquid viscosity), surface tension dominates viscous force, and a liquid drop can behave as a spring (Fig. 7). As it hits the solid, it converts a part of its kinetic energy into surface energy; after reaching a maximum size, the puddle (of diameter D_M and thickness h_m) recoils and takes off. The contact time τ is the typical response time of this liquid spring, of mass ρR^3 and stiffness γ, which yields:[12]

$$\tau \sim \left(\frac{\rho R^3}{\gamma}\right)^{1/2} \tag{7}$$

As observed experimentally, this time is on the order of 1–20 ms for millimetre-size drops. The deformation is generally large ($D_M \gg R$, $h_m \ll R$), as in Fig. 7, which means by a Weber number ($We = \rho V^2 R/\gamma$) larger than unity. This condition is easily satisfied with water since it implies impact velocities larger than 30 cm s^{-1}. For $We \gg 1$, fragments form owing to the large drop deformation; this also makes the elasticity of the shock quite modest,[12] as seen in Fig. 7 where the drop reaches after take off a height of about one millimetre, while it was released from a height of 4 cm.

The differences between spreading and recoiling are generic, in the usual cases $Ca \ll 1$ and $We \gg 1$. A convenient representation is that of Fig. 8, where we report the diameter D of the solid/liquid contact as a function of time, defining $t = 0$ as the time of contact, and $t = \tau$ as the moment of take off. Here a water drop of radius $R = 1.15$ mm hits at $V = 0.8$ m s^{-1} a superhydrophobic solid, which yields $Ca \approx 10^{-3}$ and $We \approx 10$. The solid is decorated by a square lattice of hydrophobic posts of height 24 μm, diameter 2.7 μm and mutual distance 10 μm. The graph is found to be asymmetric: in a first stage, the drop spreads very quickly on the solid; the second step is longer: after reaching its maximum expansion D_M, the liquid

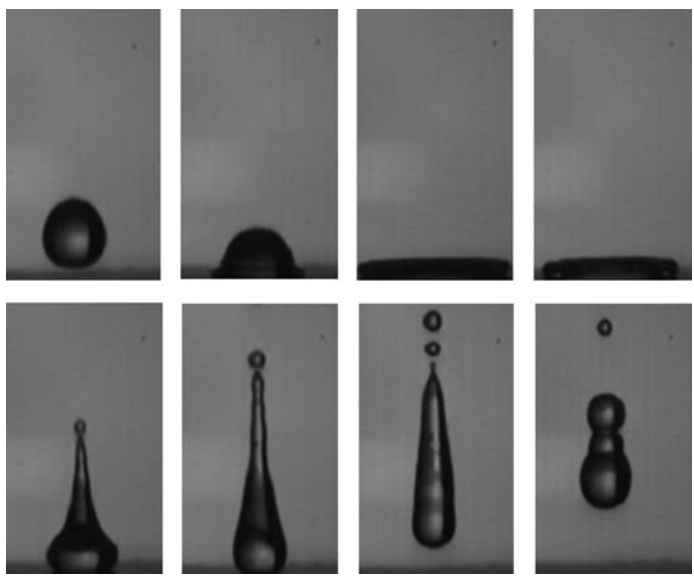

Fig. 7 Millimetric water drop impacting a super-hydrophobic solid at high Weber number $We = \rho V^2 R/\gamma$, denoting R as the drop radius, V as the impact velocity, and ρ and γ as the density and surface tension of water. Here We is 18, so that the drop gets highly elongated before taking off and emits droplets. The typical interval between successive pictures is 2 ms.

recoils at a constant dewetting velocity V_d (here of approximately 0.4 m s^{-1}) before taking off for $t > \tau \approx 13$ ms.

In the first stage (inertial spreading), the behaviour is dictated by geometry and it expresses how a solid/liquid contact establishes as a spherical drop crashes on a planar surface. In the first moments, we deduce from the geometric contact between a sphere and a plane that the size D of the contact should increase as $(RVt)^{1/2}$, where Vt is the distance of penetration of the sphere in the plane. Slightly later, the drop reaches its maximum diameter D_M and starts to recoil. The capillary force driving this stage depends on the detail of the contact: if a film of air comes between the substrate and the spreading water, then it is just 2γ (per unit length of the drop perimeter), as for a freely suspended film. It is likely that such an air cushion initially forms, but contrasting with the case of section 3, air is not constantly injected in this film, so that a static (wetting) contact may eventually set. Then, the retraction is accompanied by the creation of a new solid surface, and suppression of solid/liquid and liquid/vapour surfaces. It implies a balance of energy per unit area $\gamma_{SV} - \gamma_{SL} - \gamma$, where γ_{SV} and γ_{SL} are the effective solid/vapour and solid/liquid surface tensions in the fakir state (section 2). This yields a force per unit length $F \approx \gamma(1 - \cos\theta) \approx 2\gamma\,(1 - \varepsilon^2/4)$. Using eqn (2) (where we take $\cos\theta_o \approx 0$ for the sake of simplicity), we get: $F \approx 2\gamma\,(1 - \phi/2)$, which directly depends on the concentration ϕ of defects below the drop: the smaller ϕ, the larger the force recoiling the drop.

At low capillary numbers, viscous effects can be ignored, and the main force resisting the motion is inertia. As proposed by Taylor, Culick and Brochard-Wyart (in the context of dewetting), a rim of mass M forms at the receding edge of the puddle.[31] Newton's law expresses that $\mathrm{d}(MV_d)/\mathrm{d}t = F$; noting that $\mathrm{d}M/\mathrm{d}t = \rho h_m V_d$ (a relation again written per unit perimeter of the puddle), a solution of constant velocity is found, in agreement with the observation in Fig. 8:

$$V_d \sim \left(\frac{2\gamma}{\rho h_m}\right)^{1/2} \left(1 - \frac{\phi}{4}\right) \tag{8}$$

An explicit formula for V_d would require the knowledge of h_m, a quantity on which there is some debate. However, two remarks can be done. (i) The thickness

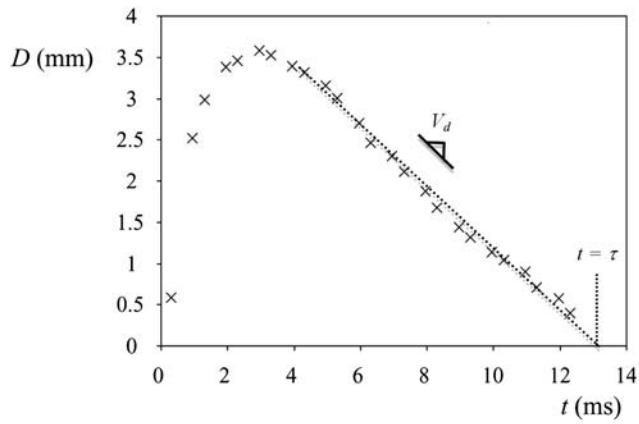

Fig. 8 Diameter D of the solid/liquid contact after a drop of radius $R = 1.15$ mm hits at $V = 0.8$ m s^{-1} a superhydrophobic solid (here $We \approx 10$), consisting of a square lattice of hydrophobic posts of height $\delta = 24$ μm, radius $b = 1.3$ μm and mutual distance $p = 10$ μm. For $We \gg 1$, spreading and retraction are asymmetric: the recoiling stage is much longer than the spreading stage, and quite linear in time.

of the pancake can be directly deduced from the observation of D_M (see Fig. 7 and 8), using volume conservation ($h_m D_M^2 \sim R^3$). From Fig. 8, for example, we deduce $h_m \approx 0.65$ mm, from which eqn (8) predicts $V_d \approx 45$ cm s^{-1}, slightly larger (yet of the same order of magnitude) than the value deduced from the figure ($V_d \approx 40$ cm s^{-1}). (ii) In the large deformation regime, the contact time is dominated by the recoiling step, that is: $\tau \sim D_M/V_d$. Using eqn (8) and volume conservation, we find, whatever the law for h_m (!): $\tau \sim (\rho R^3/\gamma)^{1/2}(1 + \phi/4)$. The contact time in eqn (7) is corrected by a function of the density of defects, a correction in qualitative agreement with the recent experiments by Li, Ma and Lan.[32] More generally, an original program of research on the dewetting on water on superhydrophobic materials (for which dewetting should be ultra-fast, due to the quasi-absence of viscous resistance) remains to be conducted. We finally note that these different laws would be slightly modified (without changing our qualitative conclusions) by the logarithmic term discussed in eqn (3).

We finally investigate a remarkable behaviour which can happen as drops impact solids decorated with posts of moderate height δ ($\delta = 18$ μm), separated by a distance $p = 10$ μm much larger than the post radius $b = 1.4$ μm (hence we deduce for these surfaces $\phi = \pi b^2/p^2 \approx 0.06$). On such dilute pillars, impact can provoke the penetration of water inside the texture, which irreversibly pins a fraction of the drop, while the rest still bounces.[13] The simplest argument we can think of for understanding the threshold in impact velocity above which penetration takes place consists of balancing the dynamical pressure at impact ρV^2 with the resisting Laplace pressure γ/p: hence, we find a velocity $(\gamma/\rho p)^{1/2}$, *i.e.* approximately 2.5 m s^{-1}. Fig. 9 shows a series of snapshots taken with a high-speed camera for an impact velocity just above this threshold ($V = 2.8$ m s^{-1}), and showing the figure of impact as seen from the top.

The impact figure exhibits original features: (i) At the place of impact, we can see a dark stain, which conveys the penetration of the drop inside the texture, where it gets irreversibly pinned. The size of the penetration zone is approximately the drop size, and it remains constant all along the sequence. (ii) A large sheet of liquid bounded by a thicker rim expands beyond this first region. Ahead of this "fakir" sheet, four fingers of liquid are emitted, in the main directions of the subjacent network of micropillars. This observation is close to what Xu *et al.* reported in similar situations, where the figure of impact was found to somehow conform to the symmetry of the underlying network.[33] Tsai and Lohse also recently did

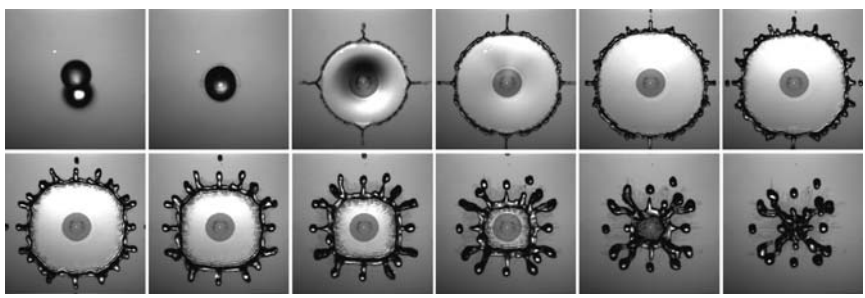

Fig. 9 Top view of the impact of a water drop of radius $R = 1.9$ mm hitting at $V = 2.8$ m s^{-1} a superhydrophobic solid decorated by a square lattice of hydrophobic posts of height $\delta = 18$ μm, radius $b = 1.4$ μm and mutual distance $p = 10$ μm. Three different effects can be observed: (i) the impact speed is large enough to provoke the penetration of liquid inside the texture, at the scale of the drop radius, as revealed by the darkening of the substrate at this place; (ii) as soon as the drop spreads inertially, four jets are emitted in the direction of the subjacent array of micropillars; (iii) in the recoiling stage, the presence of the posts induces an anisotropic dewetting, which transforms the circular drop in a quasi-square one. Interval between successive pictures: 1 ms.

comparable observations.[34] We measured the ejection speed u of these jets using very high-speed cameras, and found approximately 10 m s^{-1}. (iii) The dewetting/recoiling stage has a remarkable characteristic, namely the square shape (also reflecting the subjacent network) transiently adopted by the drop (images 1 to 4 in the second row). This pattern is reminiscent from what can be observed as making hydraulic jumps on such surfaces – then polygons similarly form.[35]

If the impact velocity is slightly increased (same substrate as in Fig. 9, same drop, but impact at $V = 2.9$ m s^{-1} instead of 2.8 m s^{-1}), an interesting variation is observed (see Fig. 10). Then, the peripheric jets also develop along the diagonals of the network, which generates an 8-fold figure of impact. The recoiling stage also seems to be characterized by the same symmetry. This phenomenon is observed for velocities up to 3.7 m s^{-1}. For still higher velocities, the impact figure becomes isotropic. Note that these figures tend to disappear gradually when decreasing the post heights; fixing this height and increasing the distance between posts broadens the window in velocity in which these "crystallographic" impacts are reported.

We do not claim to have any quantitative explanation to this phenomenon. But it seems clear that air plays a key role: the effect is observed only if the drop penetrates in the texture; then, the air present there is quickly dispelled. The volume of air brought in motion scales as $R^2\delta$, to which corresponds a flux of R^2V. Conservation of this flux implies an ejection velocity for air V_a (in the network of pillars) scaling as RV/δ, which can initially be of the order of 100 m s^{-1}! In our interpretation, the flow of air follows preferential channels, in the main directions of the network (or possibly in the diagonals) of smaller hydrodynamic resistance. This anisotropic current drags the liquid above, which results in the development of liquid filaments in the directions of the flow of air.

The drag force acting on the liquid can be in this problem either inertial, or viscous. Considering the high velocity of air, we first assume inertia to be the dominant force. As the air comes out of the network of channels, it exerts on the edge of the water film a force $\rho_a V_a^2 hR$, where h is the thickness of the liquid sheet entrained by the air. This force is mainly resisted by the liquid inertia $\rho u^2 hR$, denoting u as the liquid velocity. Using the scaling for V_a, we deduce an injection velocity:

$$u \sim \left(\frac{\rho_a}{\rho}\right)^{1/2} \frac{R}{\delta} \quad V \tag{9}$$

We expect from eqn (9) a velocity u on the order of 10 m s^{-1}, as observed experimentally. A natural criterion for observing the formation of filaments is $u > V$, which is found to be a condition on the design of the texture: $\delta < R\,(\rho_a/\rho)^{1/2}$, *i.e.* pillars smaller than approximately 30 μm. In addition, filaments can only exist if the drag force is large enough to overcome surface tension. If fingers develop on a width L, this criterion can be written: $\gamma L < \rho_a V_a^2 hL$, which can be rewritten: $V > V_c = (\gamma\delta^2/\rho_a hR^2)^{1/2}$, where V_c is expected to be typically 1 m s^{-1} for our parameters.

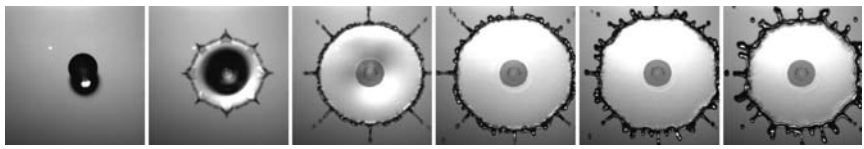

Fig. 10 Top view of the impact of a water drop of radius $R = 1.9$ mm hitting at $V = 2.9$ m s^{-1} the same superhydrophobic solid as described in Fig. 9. Eight jets are emitted, instead of four, and the drop becomes quasi-octogonal during the recoiling stage. Interval between successive pictures: 1 ms.

The viscous drag generated by the flow of air can also be significant. Considering only this drag for drawing the filament implies the force balance: $(\eta_a V_a/\delta)R^2 \sim \rho u^2 hR$, and thus an ejection velocity: $u \sim (\eta_a R^2 V/\rho h\delta^2)^{1/2}$. For our parameters, this velocity is expected to be approximately 1 m s^{-1}, smaller than above (which emphasizes that inertia might be the dominant force driving filamentation in our case). For small posts, however, viscous effects will dominate inertial ones. Then the criterion $u > V$ can be written: $\delta < R\ (\eta_a/\rho hV)^{1/2}$, which implies posts smaller than about 10 μm. Note however that very small posts would favour a viscous damping of the flow of air, thus suppressing the emission of filaments.

All these tentative ideas would need to be carefully confirmed (or not). It would be interesting to make more precise the phase diagram of these events, and in particular to understand the narrowness of the window of velocities where these crystallographic impacts are found. More generally, Fig. 9 and 10 show the possibility of (transient) coexistence between a trapped state (at the centre of the figure of impact) and a fakir state (the rest of the drop), which persists all along the sequence (so that the fakir part bounces off, while the rest of the drop remains pinned). The conditions for generating and preserving this coexistence also remain to be understood.

5. Conclusion

The aim of this paper was to put together the main and unique dynamical properties of superhydrophobic materials, when they are exposed to drops. Firstly, as noted by many authors, the contact angle hysteresis, which resists any drop motion, is minimized in this situation – and we presented a possible (quantitative) argument for understanding this fact for solids decorated by dilute pillars, a convenient model system. Secondly, the friction of water drops is dramatically reduced on these materials, compared to common solids. An original experiment was discussed, in order to stress both the very high velocities reached by the drops, and the dramatic changes in liquid shape induced by these fast motions. A few hints were given to understand the mobility of these drops, but clearly, a comprehensive experimental program remains to be conducted on this theme. Thirdly, we recalled a few features arising from drop impacts and rebounds. We also discussed how the figure of impact can reflect the presence of a texture at the solid surface, by presenting an original set of data on "crystallographic" impact, where the impact figure takes the symmetry of the underlying texture. There again, careful and complete experiments would be necessary (together with quantitative analysis) to fully capture the characteristics of these shocks.

Acknowledgements

It is a pleasure to thank Tom Witten, L. Mahadevan and Howard Stone for stimulating discussions on this topic, and Elise Bourdin for her help in the impact experiments.

References

1 J. G. Leidenfrost, *Int. J. Heat Mass Transfer*, 1966, **9**, 1153–1166.
2 T. Wagner, C. Neinhuis and W. Barthlott, *Acta Zool.*, 1996, **77**, 213–225; C. Neinhuis and W. Barthlott, *Ann. Bot.*, 1997, **79**, 667–677; X. Gao and L. Jiang, *Nature*, 2004, **432**, 36; B. Bhushan and Y. C. Jung, *Nanotechnology*, 2006, **17**, 2758–2772; E. Bormashenko, Y. Bormashenko, T. Stein, G. Whyman and E. Bormashenko, *J. Colloid Interface Sci.*, 2007, **311**, 212–216; X. F. Gao, X. Yan, X. Yao, L. Xu, K. Zhang, J. H. Zhang, B. Yang and L. Jiang, *Adv. Mater.*, 2007, **19**, 2213–2215.

3 T. Onda, S. Shibuichi, N. Satoh and K. Tsujii, *Langmuir*, 1996, **12**, 2125–2127; J. Bico, C. Marzolin and D. Quéré, *Europhys. Lett.*, 1999, **47**, 220–226; A. Nakajima, A. Fujishima, K. Hashimoto and T. Watanabe, *Adv. Mater.*, 1999, **11**, 1365–1368; D. Öner and T. J. McCarthy, *Langmuir*, 2000, **16**, 7777–7782; N. A. Patankar, *Langmuir*, 2004, **20**, 8209–8213; L. Gao and T. J. McCarthy, *J. Am. Chem. Soc.*, 2006, **128**, 9052–9053.
4 A. Lafuma and D. Quéré, *Nat. Mater.*, 2003, **2**, 457–460.
5 S. Herminghaus, *Europhys. Lett.*, 2000, **52**, 165–170; W. Chen, A. Y. Fadeev, M. C. Hsieh, D. Oner, J. Youngblood and T. J. McCarthy, *Langmuir*, 1999, **15**, 3395–3399; L. Cao, H. H. Hu and D. Gao, *Langmuir*, 2007, **23**, 4310–4314; A. Tuteja, W. Choi, M. L. Ma, J. M. Mabry, S. A. Mazzella, G. C. Rutledge, G. H. McKinley and R. E. Cohen, *Science*, 2007, **318**, 1618–1622; A. Ahuja, J. A. Taylor, V. Lifton, A. A. Sidorenko, T. R. Salamon, E. J. Lobaton, P. Kolodner and T. N. Krupenkin, *Langmuir*, 2008, **24**, 9–14.
6 C. Cottin-Bizonne, J. L. Barrat, L. Bocquet and E. Charlaix, *Nat. Mater.*, 2003, **2**, 238–240; J. Ou, B. Perot and J. P. Rothstein, *Phys. Fluids*, 2004, **16**, 4635–4643; J. Ou and J. P. Rothstein, *Phys. Fluids*, 2005, **17**, 103606; P. Joseph, C. Cottin-Bizonne, J. M. Benoit, C. Ybert, C. Journet, P. Tabeling and L. Bocquet, *Phys. Rev. Lett.*, 2006, **97**, 156104; P. Roach, G. McHale, C. R. Evans, N. J. Shirtcliffe and M. I. Newton, *Langmuir*, 2007, **23**, 9823–9830; A. Steinberger, C. Cottin-Bizonne, P. Kleimann and E. Charlaix, *Nat. Mater.*, 2007, **6**, 665–668; C. Lee, C. H. Choi and C. J. Kim, *Phys. Rev. Lett.*, 2008, **101**, 064501; F. Feuillebois, M. Z. Bazant and O. I. Vinogradova, *Phys. Rev. Lett.*, 2009, **102**, 026001.
7 J. P. Rothstein, *Annu. Rev. Fluid Mech.*, 2010, **42**, 89–109.
8 L. Mahadevan and Y. Pomeau, *Phys. Fluids*, 1999, **11**, 2449–2453.
9 D. Richard and D. Quéré, *Europhys. Lett.*, 1999, **48**, 286–291.
10 M. Miwa, A. Nakajima, A. Fujishima, K. Hashimoto and T. Watanabe, *Langmuir*, 2000, **16**, 5754–5760; M. Sakai, J. H. Song, N. Yoshida, S. Suzuki, Y. Kameshima and A. Nakajima, *Langmuir*, 2006, **22**, 4906–4909.
11 P. Aussillous and D. Quéré, *Nature*, 2001, **411**, 924–927.
12 D. Richard and D. Quéré, *Europhys. Lett.*, 2000, **50**, 769–775; D. Richard, C. Clanet and D. Quéré, *Nature*, 2002, **417**, 811–811; A. L. Biance, F. Chevy, C. Clanet, G. Lagubeau and D. Quéré, *J. Fluid Mech.*, 2006, **554**, 47–66.
13 M. Reyssat, A. Pépin, F. Marty, Y. Chen and D. Quéré, *Europhys. Lett.*, 2006, **74**, 306–312; D. Bartolo, F. Bouamrirene, E. Verneuil, A. Buguin, P. Silberzan and S. Moulinet, *Europhys. Lett.*, 2006, **74**, 299–305; P. C. Tsai, S. Pacheco, C. Pirat, L. Lefferts and D. Lohse, *Langmuir*, 2009, **25**, 12293–12298.
14 T. Deng, K. K. Varanasi, M. Hsu, N. Bhate, C. Keimel, J. Stein and M. Blohm, *Appl. Phys. Lett.*, 2009, **94**, 133109.
15 J. B. Boreyko and C. H. Chen, *Phys. Rev. Lett.*, 2009, **103**, 174502.
16 C. G. L. Furmidge, *J. Colloid Sci.*, 1962, **17**, 309–314.
17 E. B. Dussan and R. T. P. Chow, *J. Fluid Mech.*, 1983, **137**, 1–29.
18 M. Reyssat and D. Quéré, *J. Phys. Chem. B*, 2009, **113**, 3906–3909.
19 A. B. D. Cassie and S. Baxter, *Trans. Faraday Soc.*, 1944, **40**, 546–550; A. B. D. Cassie, *Discuss. Faraday Soc.*, 1948, **3**, 11–16.
20 L. Barbieri, E. Wagner and P. Hoffmann, *Langmuir*, 2007, **23**, 1723–1734.
21 P. S. Swain and R. Lipowsky, *Langmuir*, 1998, **14**, 6772–6780; G. Wolansky and A. Marmur, *Langmuir*, 1998, **14**, 5292–5297.
22 S. Brandon, A. Wachs and A. Marmur, *J. Colloid Interface Sci.*, 1997, **191**, 110–116; C. W. Extrand, *Langmuir*, 2002, **18**, 7991–7999; G. McHale, N. J. Shirtcliffe and M. I. Newton, *Langmuir*, 2004, **20**, 10146–10149; L. C. Gao and T. J. McCarthy, *Langmuir*, 2006, **22**, 6234–6237; H. Kusumaatmaja and J. M. Yeomans, *Langmuir*, 2007, **23**, 6019–6032; A de Simone, N. Grunewald and F. Otto, *Net. Heter. Med.*, 2007, **2**, 211–225; H. Kusumaatmaja and J. M. Yeomans, *Soft Matter*, 2009, **5**, 2704–2707.
23 J. F. Joanny and P. G. de Gennes, *J. Chem. Phys.*, 1984, **81**, 552–562.
24 Y. Pomeau and J. Vannimenus, *J. Colloid Interface Sci.*, 1985, **104**, 477–488.
25 K. Y. Yeh, L. J. Chen and J. Y. Chang, *Langmuir*, 2008, **24**, 245–251.
26 W. Barthlott and C. Neinhuis, *Planta*, 1997, **202**, 1–8.
27 T. Podgorski, J. M. Flesselles and L. Limat, *Phys. Rev. Lett.*, 2001, **87**, 036102.
28 E. Reyssat, F. Chevy, A. L. Biance, L. Petitjean and D. Quéré, *Europhys. Lett.*, 2007, **80**, 34005.
29 C. Duez, C. Ybert, C. Clanet and L. Bocquet, *Nat. Phys.*, 2007, **3**, 180–183.
30 O. I. Vinogradova, *Langmuir*, 1995, **11**, 2213–2220.

31 G. I. Taylor, *Proc. Roy. Soc.*, 1959, **A253**, 313–321; F. E. C. Culick, *J. Appl. Phys.*, 1960, **31**, 1128–1129; A. Buguin, L. Vovelle and F. Brochard-Wyart, *Phys. Rev. Lett.*, 1999, **83**, 1183–1186.
32 X. Li, X. Ma and Z. Lan, *Langmuir*, 2010, **26**, 4831–4838.
33 L. Xu, *Phys. Rev. E: Stat., Nonlinear, Soft Matter Phys.*, 2007, **75**, 056316; L. Xu, L. Barcos and S. R. Nagel, *Phys. Rev. E: Stat., Nonlinear, Soft Matter Phys.*, 2007, **76**, 066311.
34 P. C. Tsai and D. Lohse, personal communication (2010).
35 E. Dressaire, L. Courbin, J. Crest and H. A. Stone, *Phys. Rev. Lett.*, 2009, **102**, 194503.